Dalton Transactions

Accepted Manuscript

ROYAL SOCIETY OF CHEMISTRY

www.rsc.org/dalton

Oleylamine as a beneficial agent for the synthesis of $CoFe_2O_4$ nanoparticles with potential biomedical uses

Violetta Georgiadou,[a] Chrysoula Kokotidou,[b] Benjamin Le Droumaguet,[c,d] Benjamin Carbonnier,[c,d] Theodora Choli-Papadopoulou[b] and Catherine Dendrinou-Samara*[a]

[a]Department of Inorganic Chemistry, Aristotle University of Thessaloniki, 54124 Thessaloniki, Greece; [b] Department of Biochemistry, Aristotle University of Thessaloniki, 54124 Thessaloniki, Greece; [c]Institut de Chimie et des Matériaux, Paris-Est (ICMPE)-UMR 7182, Equipe Systèmes Polymères Complexes (SPC) 2-8, rue Henri Dunant 94320 Thiais, France ; [d]Université Paris-Est Créteil Val-de-Marne, Faculté des Sciences 61, Avenue du Général de Gaulle 94010 Créteil Cedex

* Corresponding author, Email: samkat@chem.auth.gr, Tel: +30-2310-99-7876

Abstract

The multifunctional role of oleylamine (OAm) as a versatile and flexible reagent in synthesis as well as a desired surface ligand for the synthesis of $CoFe_2O_4$ nanoparticles (NPs) is described. $CoFe_2O_4$ NPs have been prepared by a facile, reproducible and scalable solvothermal approach in the presence of pure OAm. By monitoring the volume of OAm, different shapes of NPs, spherical and truncated were formed. The syntheses led to high yields of monodispersed, considerably small (9-11nm) and with enhanced magnetization (M_s= 84.7-87.5 emu/g) $CoFe_2O_4$ NPs. The resulted hydrophobic $CoFe_2O_4$ NPs were easily transferred to an aqueous phase through the formation of reverse micelles between the hydrophobic chains of OAm and cetyltrimethylammonium bromide (CTAB) and transverse relaxivities (r_2) were measured. The spherical NPs had the greater effect on water proton relaxivity (r_2= 553 $mM^{-1}s^{-1}$) at an applied magnetic field of 11.7 T. The NPs became fluorescent probes by exploiting the presence of the double bond of OAm in the middle of the molecule; a thiol-ene "click" reaction with the fluorophore bovine serum albumin (FITC-BSA) was achieved. The labeled/biofunctionalized $CoFe_2O_4$ NPs interacted with cancer (HeLa and A549) and non-cancer cell lines (MRC5 and Dental MSCS) and cell viability was estimated. A clear difference of toxicity between the cancer and non-cancer cells was observed while low cytotoxicity in living cells was supported. Confocal laser microscopy showed that NPs entered the cell membranes and were firstly localized close to them provoking a membrane expansion and were further accumulated perinuclear without entering the nuclei.

Keywords: oleylamine, $CoFe_2O_4$ nanoparticles, solvothermal, relaxivity, thiol-ene "click" reaction

Introduction

Spinel ferrite nanoparticles, MFe_2O_4 (M = Mn, Co, Ni, Fe, etc.) is a class of inorganic oxide nanoparticles with remarkable magnetic properties that offer a broad spectrum of applications.[1] The most popular representative members, superparamagnetic iron oxide (SPIO) and ultra small superparamagnetic iron oxide (USPIO) nanoparticles have already been proposed/used for bioapplications.[2] Nowadays, cobalt or manganese ferrite nanoparticles (NPs) are investigated thoroughly as better candidates in therapy and diagnosis, (so-called theranostics), than magnetite or maghemite NPs mostly due to their improved magnetic properties.[3] In particular, cobalt ferrite NPs ($CoFe_2O_4$ NPs) are studied as enhancement agents of signal reception in magnetic resonance imaging (MRI), hyperthermia agents since they offer finer heating absorption capacity and magnetically tagging devices of bioentities, for bioseparation and drug delivery.[4] Each of these applications requires NPs with specific characteristics, such as desired sizes, modified surface and narrow polydispersity in aqueous media.[5] Wet chemistry approaches in organic solvent have been proven highly efficient for controlling these characteristics.[6] However, there is still a demand to develop simple, inexpensive, reproducible NPs for large-scale preparation of high quality nanoparticles with specific properties able for multiple bioapplications such as theranostics.

Herein, a facile solvothermal synthesis of $CoFe_2O_4$ NPs is described in the presence of pure oleylamine (OAm). OAm has been selected for the preparation based on its multifunctional role: it is a long chain primary alkylamine acting as reducing agent and electron donor in high temperatures; liquid in room temperature with high boiling point (348-350 °C) that allows a high temperature wet route to be carried out and it is easily manipulated through the washing procedure that follows the separation of the NPs. Meanwhile, the presence of the double bond in the middle of the molecule offers a bending configuration that enhances its coordination ability towards the metal core.[7] Recently a review by Mourdikoudis and Liz-Marzan covers the role of OAm in NPs syntheses, illustrated all the important aspects in the formation of noble metal NPs, semiconductors and transition metal oxide NPs through different synthetic methods.[8] Nevertheless, and to the best of our knowledge there are only two recent reports where it has been used as the main surfactant to support syntheses of MFe_2O_4 NPs through a thermal decomposition preparation[9] while further utilization of OAm has never been reported.

Aside from the original synthetic procedure and product characterization, an investigation of the prepared $CoFe_2O_4$ NPs as candidates for theranostics was undertaken. Thus, in order to study whether the synthesized NPs can affect/increase the relaxivity of water protons, the as prepared hydrophobic $CoFe_2O_4$ NPs were modified to hydrophilic via a reverse micelle method and relaxivity measurements were carried out via NMR measurements. Meanwhile, by taking advantage of OAm double bond on the surface of $CoFe_2O_4$ NPs, a thiol-ene reaction[10] was attempted with a fluorescein isothiocyanate labeled bovine serum albumin (FITC-BSA) molecule in order to study their behavior in vitro. This mild reaction, from the so-called "click" type, allows in general the specific coupling of organic, macromolecular as well as biological or inorganic templates in a straightforward fashion while tedious purification are not required to provide the final product. It proceeds through the addition of a thiol-containing compound to an olefin via a radical or ionic mechanism. In that way, $CoFe_2O_4$ NPs were coated with FITC-BSA. The functionalized NPs as well as pure OAm were further investigated for their in vitro toxicity by using 3-(4,5-dimethyl-2-thiazolyl)-2,5-diphenyl-2H-tetrazolium bromide (MTT) assays on both non-cancer immortalized (MRC5 (human fetal lung fibroblast), Dental MSCS (mesenchymal stem cells derived from dental tissues) and cancer human cells lines (A549

(human pulmonary carcinoma cell line), HeLa (human epithelial carcinoma cell line)). MTT assays showed a distinct variation of cell viability between cancer and non-cancer cell lines. In addition, their cytoplasmic localization and association with cell nuclei have been probed into by confocal laser microscopy.

Experimental Section

Chemicals: Iron (III) acetylacetonate (≥ 97.0%, $Fe(acac)_3$, Fluka). Cobalt (III) acetylacetonate (≥ 99.9%, $Co(acac)_3$), deuterated chloroform-d_1 (99.5%), sodium chloride (NaCl), magnesium chloride ($MgCl_2$), ethyleneglycol-*bis*(β-aminoethyl)-N,N,N′,N′-tetraacetic acid **(**EGTA), phenylmethylsulfonyl fluoride **(**PMSF), sodium dodecyl sulphate (SDS) were all from Merck. Oleylamine (technical grade, 70%, OAm), 2,2-dimethoxy-2-phenylacetophenone (DMPA, 99%), fluorescein isothiocyanate labeled bovine serum albumin (FITC-BSA), propidium iodide (PI), formaldehyde solution, RNAse were provided by Sigma Aldrich. Dimethylsulfoxide (DMSO), chloroform ($CHCl_3$) (Chem. Lab NV). Cetyltrimethylammonium bromide (CTAB, 98%, Alfa Aesar). Deuteriumoxid (D_2O, 99.9%, Deutero GmbH). Ethanol (100%, 1% MEK, Bruggermann GmbH). Tissue culture coverslips 13mm (Sarstedt). Microscope slides, Superfrost (O. Kindler GmbH). Culture medium DMEM (Dulbecco's modified eagle medium with L-glutamin), fetal bovine serum (FBS), Antibiotic-Antimycotic, PBS (pH=7,2) (E.U Gibco BRL). Trypsin+EDTA, 3-(4,5-dimethylthiazol-2-yl)-2,5- diphenyltetrazolium bromide (MTT powder) (Invitrogen). All reagents were used without any further purification.

Preparation of $CoFe_2O_4$ NPs: Three experiments were conducted named CoFerrite1-3. CoFerrite1 was prepared by dissolving 1.8 mmol of $Fe(acac)_3$ and 0.9 mmol of $Co(acac)_3$ in 16 mL of OAm. For CoFerrite2 1.8 mmol of $Fe(acac)_3$ and 0.9 mmol of $Co(acac)_3$ were dissolved in 6 mL of OAm and for CoFerrite3, 0.9 mmol of $Fe(acac)_3$ and 0.9 mmol $Co(acac)_3$ were dissolved in 16 mL of OAm. The reddish homogeneous solutions were sealed in Teflon-lined steel autoclaves (23 mL capacity) without degassing the solutions, and were heated up with a stable rate of 4 °C/min until temperature reached 200 °C; temperature remained stable for 24 h. After a 24 h reaction, the Teflon lined bombs were left to cool down to room temperature at a stable rate of 5°C/min and $CoFe_2O_4$ NPs were obtained after several washes with ethanol by centrifugation at 5000 rpm for 15 min and dried under vacuum.

Surface modification with cetyltrimethylammonium bromide: The hydrophobic surface of the as prepared CoFerrite1 and CoFerrite2 has been modified to hydrophilic according to an alternative version of a procedure reported in literature[11]. In this way, 3 mg of as prepared NPs CoFerrite1 and CoFerrite2 were dissolved in $CHCl_3$ and sonicated for 5 min. A solution of CTAB (0.02 M) in 10% D_2O/milli pure water was prepared and sonicated until it became transparent. The two solutions were added together and were sonicated for several hours, until the chloroform evaporated from the system and the solution became limpid. The resulting solution (0.9 mM metal ions (Fe+Co)@CTAB/water) was used as stock in order to prepare a series of diluted solutions, ([Fe+Co]: 0.8, 0.6, 0.4, 0.2 mM). Metal ion concentration of the stock solution was determined by ICP-OES and EDS method analysis.

Reaction with fluorescein isothiocyanate labeled bovine serum albumin: For the thiol-ene reaction of NPs with FTIC-BSA, 10.9 mg of desiccated CoFerrite2 NPs and 10.5 mg of FITC-BSA were separately dissolved in 5 mL DMSO by vigorous shaking and were then joined

together (10 mL total reaction mixture). A solution of 5 mg DMPA (photoinitiator) in 1 mL DMSO was prepared and 100 μL of this latter were finally added in the reaction mixture. The mixture was shaken vigorously in order to obtain a homogeneous suspension and it was placed in a UV oven (Spectrolinker) for 2 h irradiating with a fixed wavelength of 365 nm. The resulting suspension was centrifuged for 10 min at 14000 rpm. Once the supernatant was discarded, the pellet was re-suspended in DMSO or milli-pure water. This centrifugation cycle was repeated at least twice in order to afford the pure FITC-BSA coated magnetic nanoparticles (CoFerrite2@FITC-BSA).

Cell culture: Human cell lines from four different sources, namely A549, immortalized MRC5, HeLa, and Dental MSCS were cultured in DMEM supplemented with 10% FBS and antibiotics penicillin and streptomycin. Cell line was maintained in continuous culture at 37 ^{o}C, in 5% CO_2, in a fully humidified incubator, using standard aseptic techniques and cell growth was monitored by determining the cell number/ with the use of a Coulter counter model ZBI.

MTT assays: Cell proliferation was assessed by monitoring the conversion of 3-(4,5-dimethyl-2-thiazolyl)-2,5-diphenyl-2H-tetrazolium bromide (MTT) to formazan. The reduction of MTT is catalyzed by mitochondrial dehydrogenase enzyme and is therefore a measure for cell viability[12]. The MTT assay was used as a cytotoxicity assay for the above cells lines grown in the presence of the studied compounds. Briefly, cells with concentrations of $1x10^4$ cells/well (A549 and Dental) and $5x10^3$ cells /well (HeLa and MRC5) were seeded in 96-well plates and after 24 h were treated with varying amounts (5, 10, 20, 30, 50, 80, 100 and 150 μg/mL) of the NPs suspended in the culture medium mentioned above. Cells which were not exposed to NPs served as control. The NPs incubation with the cells for 48 h and was followed by medium removal from each well and its replacement with 100 μL fresh medium and 10 μL MTT 20 mM (5 mg/mL) per well. After another short incubation for 4 h at 37 °C until the development of the purple colored formazan product, 100 μL of SDS 10%-HCl 0,01M were added to the cells, which were left under the same growth conditions for 15-18 h. The Organon Teknika@ Enterprise Ireland plate was used to measure the absorbance of the plates at 570 nm. The values shown are ensued after three measurements, namely each indicated point represents mean of three wells.

Propidium iodide staining and confocal microscopy studies: The intracellular localization of CoFerrite2@FITC-BSA NPs was investigated by measuring their emitted fluorescence within the pretreated cells in a coupled nuclei staining procedure with PI[13] as described below: $5x10^4$ cells from the Dental MSCS were left to attach for 24 h on the small round glass (Tissue Culture Coverslips 13 mm) placed in each well of a 6-well plate (Corning Inc) that was pre-filled with 2 of DMEM growth medium. After the incubation 10 μL of NPs suspension (1mg/mL in DMSO) were added to each well and left for 48 h to incubate under the same conditions, namely 5% CO_2 and 37 °C, and followed by growth medium removal and PBS wash (2 times). After that cells were fixed by using 1% formaldehyde in PBS for 5 min, washed with PBS, covered with Quench buffer (Tris-HCl PH 7.5 1M, PBS 1x), that was discarded after 5 min, and washed again with PBS. The immobilized cells were left for 12 min in the permeabilization buffer (150 mM NaCl, 100 mM Tris-HCl Ph 7.5, 2 mM $MgCl_2$, 0.2% TX-100, 0.5% gelatin, 0.1 mM EGTA, 0.5 Mm PMSF) followed by a quick wash with blocking buffer (permeabilization buffer without PMSF) and a second wash with PBS. The round glasses were removed from the well and RNAse

(1mg/mL in PBS) was added. After 30 min addition, a wash with PBS followed and addition of PI at a concentration of 1:200. The cells were washed with PBS (x3) and post-fixation was performed using a 4% formaldehyde solution. Thereafter the glasses were washed with PBS again and mounted onto a microscope slide for confocal laser microscopy.

Measurements: Powder X-ray diffraction (XRD) was performed using a 2-cycle Rigaku Ultima + diffractometer (40 kV, 30 mA, CuKα radiation) with Bragg-Brentano geometry (detection limit 2% approximately). TEM images, JEOL 100 CX microscope (TEM), Philips CM12 transmission electron microscope (80 kV at acceleration voltage of 100 kV). Elemental analysis was tested by inductively coupled plasma optical emission spectroscopy (ICP-OES, ICP Simultané VARIAN Vista Axial) and Energy dispersive detector (EDS) integrated to a scanning electron microscopy instrument (SEM), JEOL 840A. Fourier transform infrared (FT-IR) spectroscopy (280-4000 cm^{-1}) was recorded using a Nicolet FTIR 6700 spectrometer (samples prepared as KBr pellets). Thermogravimetric analysis (TGA), SETA-RAM SetSys-1200 (heating rate of 10 $^0C\ min^{-1}$, N_2). Magnetic measurements, Superconducting Quantum Interference Device (Quantum Design MPMS-5 SQUID) and Vibrating Sample Magnetometer (1.2H/CF/ HT Oxford Instruments VSM). T_2 transverse relaxation time measurements and ^{1}H-NMR spectra were carried out at a 500-MR NMR Spectrometer (500 MHz, Agilent Technologies) (11.7 T applied), Carr-Purcell-Meiboom-Gill (CPMG) pulse sequence. DLS measurements by Malvern Zetasizer. Bradford method, Jenway 6305 UV/Vis Spectrophotometer (595 nm). Fluorescence measurements, Hitachi F-7000 Fluorescence spectrophotometer (emission spectra at 500 nm). Confocal Laser Microscopy, Nikon D-eclipse, data were manipulated by EZC1 320, Nikon software. Graphite Furnace Atomic Absorption Spectrometry (GFAAS) for Fe was measured at a Perkin Elmer HG 900 Graphite Furnace, Fe standard: Panreac Fe=1000 ± 0.002 g/L.

Results and Discussion

Synthetic aspects

Solvothermal synthesis of $CoFe_2O_4$ NPs was carried out successfully by dissolving anhydrous $Fe(acac)_3$ and $Co(acac)_3$ in pure OAm. In all samples, OAm can be considered a crucial reagent, acting in diverse ways in the preparation; solvent, reducing agent and surfactant, yielding hydrophobic NPs. Meanwhile, OAm can provide a desired surface chemistry and functionality and yet survives the harsh reaction conditions. The starting volume of OAm in the closed bombs varied in order to examine how the autogenous pressure created by the enclosed atmospheric air, affected the resulting NPs.[14] In general pressure has great impact in solvothermal synthesis. High pressure affects the formation of products as previously reported by modifying the formation energy value.[15] This energy is directly correlated to the compressibility of the involved medium, a value that is very important in case of gases, while it is less important in case of liquids and solids. A liquid can enhance a solvothermal reaction by meliorating the solubility of chemical species in the medium and by decreasing the distance between them, the liquid/solid interaction can be improved. Thus, in the case of CoFerrite2, ~26% of the reaction vessel was filled with liquid (6 mL OAm), whereas for CoFerrite1, ~70% of the capacity was covered with OAm and in that way atmospheric air was less in the vessel. Consequently, CoFerrite1 was prepared under lower pressure than CoFerrite2. Moreover, the role of the precursors ratio in composition was examined in case of CoFerrite3, where 1Co:1Fe ratio was used instead of the formulation requirement (1Co:2Fe). In all cases (CoFerrite1-3) the proposed formation mechanism of the spinel, is analogous of what Niederberger *et al.*[16] reported

previously. Formation of the spinel ferrites commences with a solvolysis of the acetylacetonate species followed by ketimine condensation reactions resulting in cobalt and iron hydroxides while after their dehydration, formation of $CoFe_2O_4$ nanoparticles occurs.

Characterization

The structural characterization and magnetic properties discussed in this section are summarized in **Table 1**. Bragg reflections in the 2θ range of 10-90° confirmed the formation of Cobalt Ferrite phase in all samples (**Figure 1**) (PDF card no.22-1086). The characteristic peaks of the cubic spinel structure Fd3m (227) were evident, whereas in the pattern of CoFerrite3 a small amount of a second phase was observed, attributed to CoO (PDF card no.48-1719). Lattice parameters for the spinel phase were calculated, 8.403(0) Å, 8.393(0) and Å 8.403(0) Å for CoFerrite1, CoFerrite2 and CoFerrite3 respectively and were found close to the bulk value (a=8.392(1) Å).

Table 1. Structural and magnetic properties of $CoFe_2O_4$ NPs

Sample	Phase By XRD	Size XRD (nm)	Size TEM (nm)	Lattice parameter (Å)	M_s (emu/g)	M_s (emu/g) On the effective mass	H_c (Oe)
CoFerrite1	$CoFe_2O_4$	9.2(1)	9	8.403(1)	63.6	84.7	247
CoFerrite2	$CoFe_2O_4$	9.6(1)	10.7	8.393(1)	63.0	87.5	370
CoFerrite3	$CoFe_2O_4$ (86%) CoO (14%)	6.1(3) 27.4(4)	5.3 26.7	8.403(1) 4.273(0)	34.0	56.8	192

In general, NPs are expected to have smaller lattice parameters than the bulk due to nanosize effects; however the slight increment in case of CoFerrite1 and CoFerrite3 can be attributed to lattice expansion as a result of the interfacial energy and mutual surface tension attraction. This behavior can be thermodynamically enlightened during the nucleation and growth process of the NPs[17] and as a result when the average particle size decreases, both lattice parameters and the unit cell volume become larger. The average crystalline size was calculated by fitting the diffraction data and by using a pseudo-Voigt function (Jade6 Software). Sizes for CoFerrite1 and CoFerrite2 were found 9.2(1) nm and 9.6(1) nm respectively. Intensity peaks between the two XRD patterns slightly differ, causing an unequal full width at half-maximum (FWHM) and consequently a small deviation of the average crystalline size. This deviation could be attributed to the different starting volume in the closed bomb.

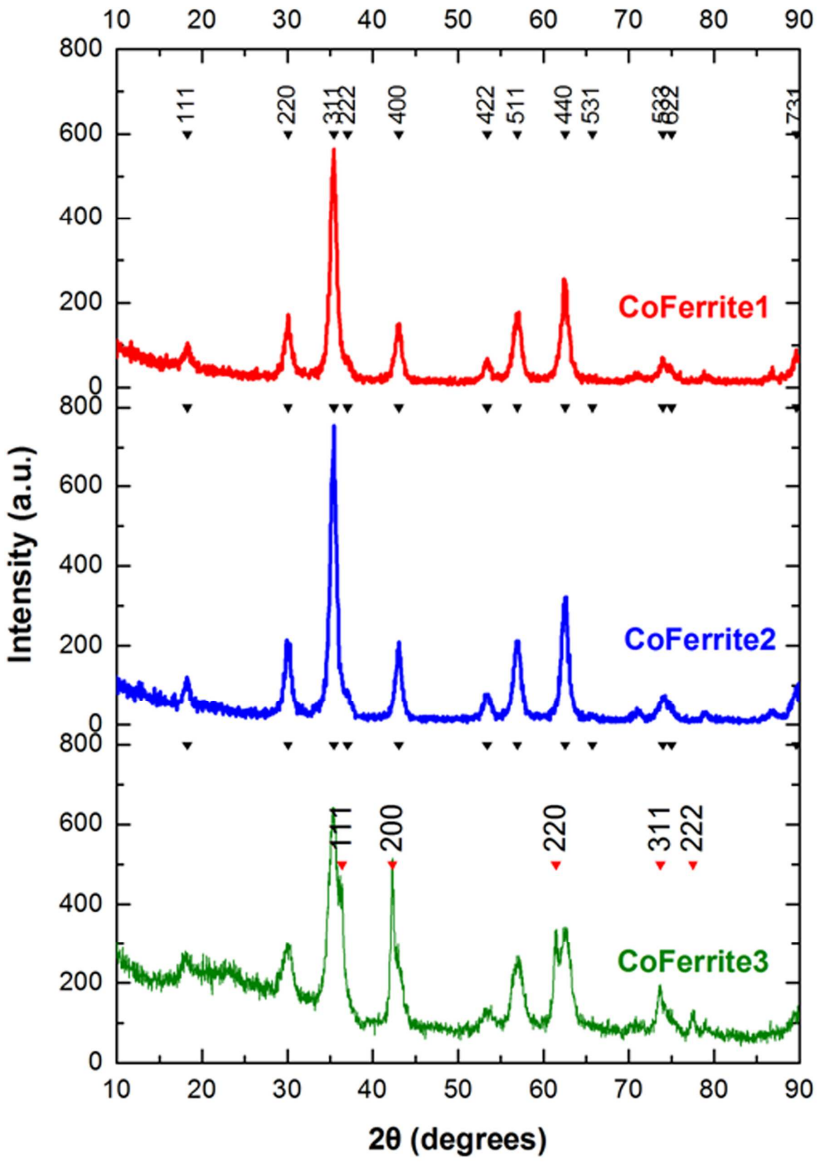

Figure 1. X-Ray diffraction diagrams of $CoFe_2O_4$ NPs (▼$CoFe_2O_4$, ▼ CoO)

TEM images of CoFerrite1 and CoFerrite2 are shown in **Figure 2a** and **b** respectively and for CoFerrite3 the image can be found in **Fig.1S**. It can be observed that CoFerrite1 consists mainly of small and spherical NPs, while CoFerrite2 is a mixture of cubic and polygonal NPs favored by the higher-pressure conditions. Meanwhile for CoFerrite3, apart from a small sized spherical phase (5.3 nm), a bigger cubic-shaped phase is observed. It is assumed that the large cubical nanoparticles correspond to CoO phase (**Fig.1S**), based on the XRD size calculations as CoO phase showed size of 26.7 nm and were the only big nanoparticles in the assembly. Statistical analyses for each sample by counting 196 NPs were fitted with a standard Log-Normal function and sizes were found 9.0 ± 3.8 nm and 10.7 ± 2.4 nm for CoFerrite1 (**Figure 2a**) and CoFerrite2 (**Figure 2b**) respectively. Although the sizes are similar, size distribution was found quite different, for comparison the overlapping of the size distributions is given in ESI, indicating lower monodispersity of CoFerrite1 than that of CoFerrite2 (**Fig2S**).

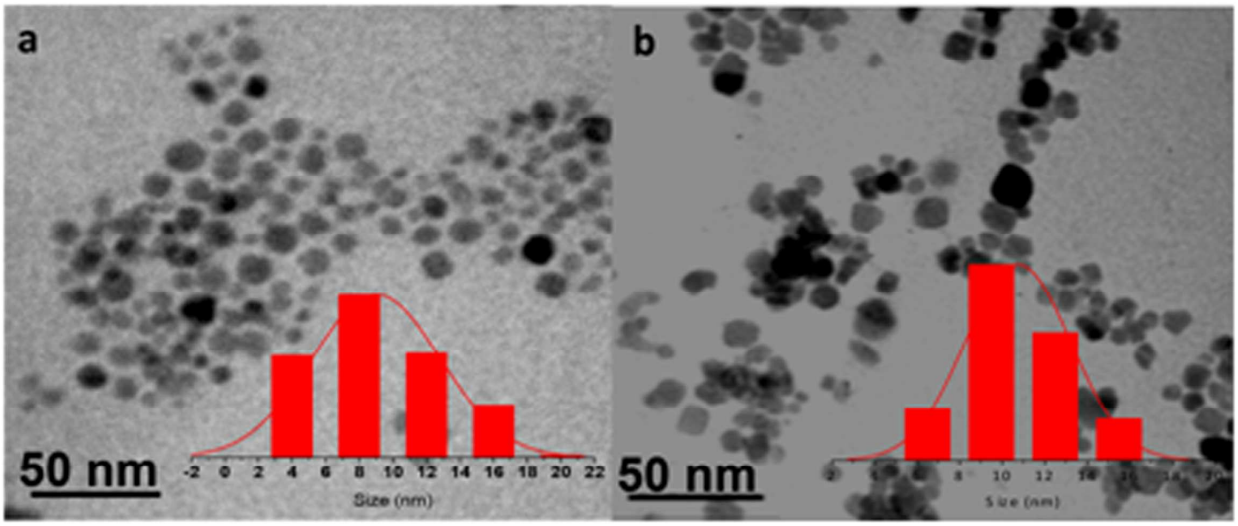

Figure 2. TEM images of a) CoFerrite1, b) CoFerrite2

The FT-IR spectra of the samples (**Figure 3a**) showed all the characteristic peaks of OAm[18]. The high frequency bands observed in the region 2923 cm^{-1} and 2854 cm^{-1} are attributed to the ν_{as} and ν_s stretching vibrations of methylene groups ($-CH_2$) respectively, while the small intensity peak at 3001 cm^{-1} is attributed to =C-H. The shoulder at 1641 cm^{-1} is characteristic of the double bond (C=C) of OAm, and has low intensity because of the sterical inhibition of the molecule[19]. The peaks at 1557 and 722 cm^{-1} are attributed to NH_2 group and are found shifted to some extent, due to Van der Waals interactions with the metal core. Peaks below 700 cm^{-1} are attributed to the spinel structure; ν_1 is detected at 584 cm^{-1} and ν_2 at 390 cm^{-1}. These two modes correspond to the motion of oxygen with respect to the tetrahedral and octahedral cations in the spinel cell.[20] TGA curves (**Figure 3S**) demonstrate the weight loss over a temperature rate of 200-700 °C, due to the decomposition of OAm. The total weight loss of the two samples found similar, 26% and 28% for CoFerrite1 and CoFerrite2 respectively.

Magnetic properties of the NPs were measured on a VSM (**Figure 3b**). The obtained values on the effective mass (values after correction by TGA data), were 84.7 and 87.5 emu/g for CoFerrite1 and CoFerrite2 respectively, while for CoFerrite3 a reduced M_s value was observed as expected (56.8 emu/g) due to the smaller size (6.1 nm) and secondarily because of the coexistence of the second phase (CoO, 17%, percentage calculated by Jade6 Software).

These values were in good agreement with the expected ones for stoichiometric bulk $CoFe_2O_4$ (80.8 emu/g)[21] and were among the highest for small sized NPs when compared to results reported in literature *eg.*74.10 emu/g (value corrected by TGA data)[22] and 60.59 emu/g (net magnetization value)[23]. The enhancement of magnetization is attributed to oxygen vacancies in the spinel that can reduce the dead layer (spin disorder layer structure) as it has been previously described by Yang *et al.*[24] and can result in values comparable or higher than the bulk. A similar behavior has been observed for $NiFe_2O_4$[25] and $ZnFe_2O_4$[26]. Furthermore, decrease of the dead layer can also be induced by the coordination of OAm on the metal core as J. Mohapatra *et al.*[9] has suggested recently for NPs larger than 4 nm. OAm as an σ-donor increases

the spin-orbit coupling due to a decrease of the crystal field splitting and therefore favors the uplift of the magnetocrystalline anisotropy of the surface layer.

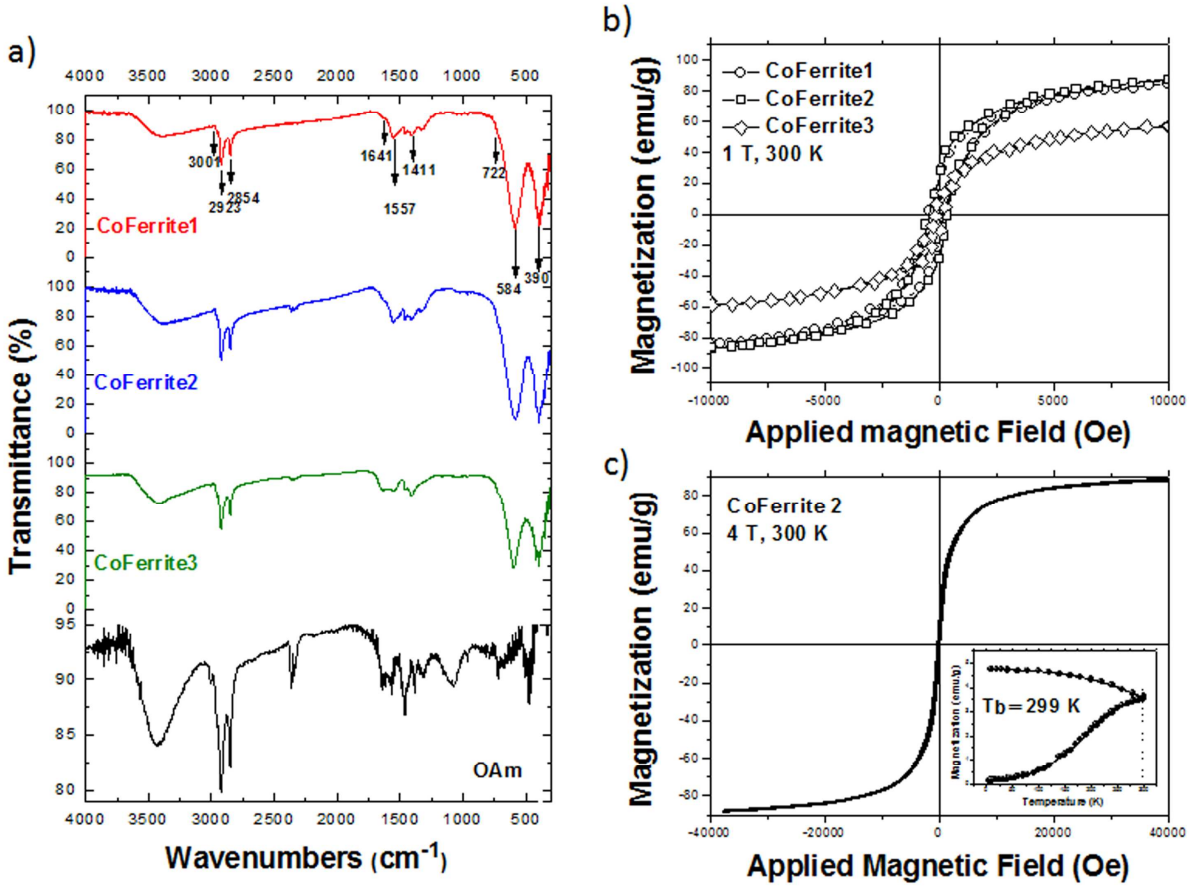

Figure 3. a) Infrared spectra of CoFerrite1(red), CoFerrite2 (blue), CoFerrite3 (green) and pure OAm (black), b) VSM measurements on the effective mass of samples CoFerrite1 (-○-), CoFerrite2 (-□-) and CoFerrite3 (-◇-) c) SQUID measurement of sample CoFerrite2 (4 T, 300 K), inset: ZFC and FC measurement

Coercivity field (H_c) increased from CoFerrite1 (247 Oe) to CoFerrite2 (370 Oe) The presence of a large coercive field (Hc) in case of cobalt ferrites is based on[27-29]: surface anisotropy (surface/volume ratio); shape anisotropy (polygonal, truncated NPs have larger anisotropy compared to spherical ones); the chemical identity of cobalt due to-the large orbital contribution to the magnetic moment and finally the particle size, which is directly correlated to the coercive field (Hc). Taking into account that CoFerrite1 and CoFerrite2 have almost similar sizes and are both capped with OAm different coercivity values are attributed to shape anisotropy as truncated nanoparticles (CoFerrite2) have larger anisotropy compared to spherical ones (CoFerrite1) in accordance with literature.[27]

Additionally, SQUID measurements were carried out for CoFerrite2 (**Figure 3c**) in proportion with zero field cooling (ZFC) and field cooling (FC) measurements (**Figure 3d**) as this sample has been further investigated for bioapplications.[30] ZFC/FC measurements showed that the sample is in a ferrimagnetic state below T_b (T_b= 299 K), whereas paramagnetic behavior is not observed above T_b following the Curie-Weiss law with decreased magnetization as the NPs remain in a blocked ferrimagnetic state at room temperature.[29]

Relaxivity

Spinel ferrite NPs have been proposed previously as T_2 transverse (spin-spin) contrast agents in MRI[31]. When the NPs are dispersed in aqueous medium under the influence of a magnetic field they can induce local magnetic field inhomogeneities and evoke the decrease of T_2 transverse relaxation time of the nearby water protons. The consequence of this decrease is the weakening of signal intensity (darker images in MRI), with a certain R_2 rate with respect to the metal ions concentration (C) of the aqueous solution of NPs (**Eq. 1**).[32] Relaxivity, r_2 is the slope of the fitting curve of the different points in the plot of concentration (C) against R_2 (C,R_2).

$$R_2 = \frac{1}{T_2} = \frac{1}{T_2^0} + r_2 C \quad , \qquad \textbf{Eq. 1}$$

In order to study if the prepared hydrophobic $CoFe_2O_4$ NPs can act as candidates for T_2 contrast imaging, relaxivity measurements were taken out in a 500-MR NMR spectrometer. The as prepared NPs were converted to hydrophilic with CTAB via a reverse micelle method in order to form stable aqueous dispersions. T_2 transverse relaxation time was measured for four different concentrations (C= 0.8, 0.6, 0.4, 0.2 mM) (**Figure 4**) and transverse relaxivity values (r_2) of water protons were calculated [32] (**Eq. 1**). In spite of the considerably similar size and magnetization of the samples in the present study, CoFerrite1 gave a notably higher r_2 value (553 $mM^{-1}s^1$) compared to CoFerrite2 (239 $mM^{-1}s^{-1}$) (**Figure 4**). Since the general notion is that r_2 increases with increasing size or with increasing saturation magnetization[32] CoFerrite1 and CoFerrite2 would be expected to have a similar effect on relaxivity or even larger for sample CoFerrite2 due to the shape factor (spherical and truncated) that Joshi *et al.*[23] had reported. DLS measurements showed that the aqueous dispersion of CoFerrite2 (0.2 mM CTAB/H_2O) has a 353 nm hydrodynamic diameter, suggesting a strong inhibition of interaction between the metal core and the water protons. On the other hand, CoFerrite1 (0.2 mM CTAB/H_2O) was found to have a smaller hydrodynamic size (193 nm) and actually has a larger effect on relaxivity (r_2=553 $mM^{-1}s^{-1}$). Reverse micelle method that has been used to alter the solubility as a qualitative approach resulted to a different hydrophilic coating although OAm participates in the same percentage in both samples (26% and 28%). CoFerrite1 formed a better aqueous colloidal dispersion with CTAB than CoFerrite2 under the conditions used, yet both samples affected relaxivity in a positive way and afforded with higher r_2 values than the one reported previously for 10 nm maghemite NPs (r_2 = 228 $mM^{-1}s^{-1}$) (11.7 T, 500 MHz spectrometer)[33] while Aslam *et al.*[34] found a range of $r_{2=}$ 80-232 $mM^{-1}s^{-1}$ (60 MHz) for magnetite NPs with sizes 29-39 nm and Joshi *et al*[23] reported for spherical $CoFe_2O_4$ NPs with sizes 6-15 nm (metal core size), a range of r_2 values 110.9-301.8 $mM^{-1}s^{-1}$, whereas for faceted $CoFe_2O_4$ NPs with sizes 12 nm and 25 nm, r_2 was 150.1 $mM^{-1}s^{-1}$ and 345.2 $mM^{-1}s^{-1}$ respectively (GE Sigma 3.0 HDxt MR system).

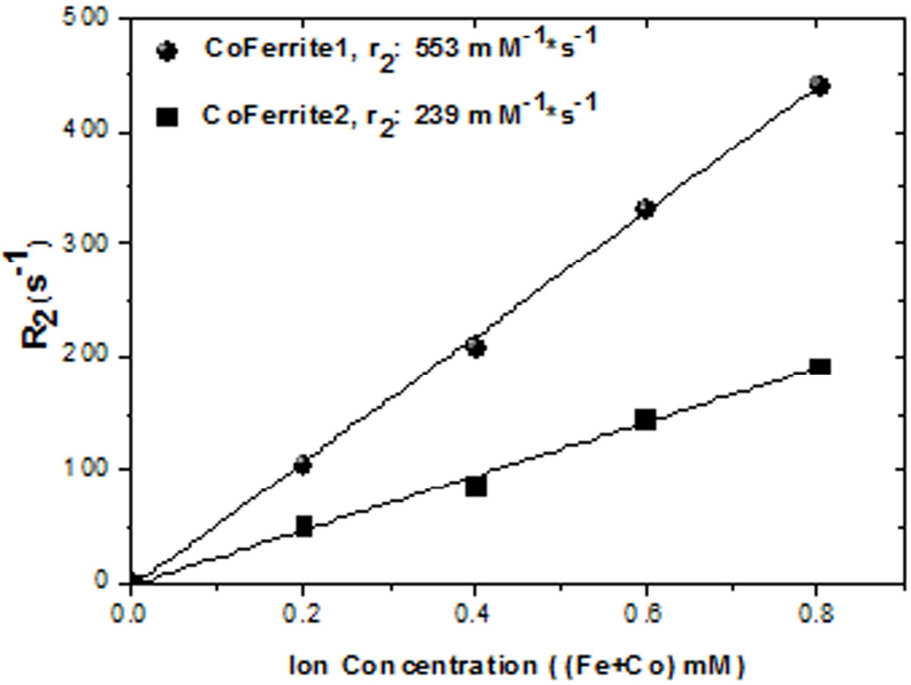

Figure 4. r_2 transverse relaxivity of water protons by samples CoFerrite1 (●) and CoFerrite2 (■) measured at 11.7 T in a 500-MR NMR Spectrometer

Fluorescence Probes/Functionalization with FITC-BSA

$CoFe_2O_4$ NPs coated with silica have been proposed before as fluorescent probes mainly through functionalization with rhodamine and to some degree with other dyes (RITC, FITC).[35] Herein, a conjugate of fluorescein isothiocyanate (FITC) with bovine serum albumin (BSA) was used for the functionalization of OAm coated $CoFe_2O_4$ NPs in order to preserve in advance the biocompatibility of the NPs. Albumin NPs have been thoroughly investigated as effective delivery systems in nanomedicine.[36] BSA has been proposed as a successful alternate of human serum albumin nanocarrier for applications in nanomedicine due to the possibility to coat lipophilic NPs.[37] In addition, photochemically-driven thiol-ene "click" strategy is a very efficient, mild and simple chemical reaction, without side products and proceeding rapidly to high yield.[38] It is well known that under UV-light thiol groups can generate thiyl radicals which are highly reactive towards C=C double bonds.[39] Therefore, UV activation was selected in order to covalently anchor the FITC-BSA at the surface of CoFerrite2 NPs. The first evidence of the successful reaction comes from the comparison of the FT-IR spectra of the as prepared CoFerrite2 NPs, pure FITC-BSA and the coated $CoFe_2O_4$@FITC-BSA NPs (**Figure 5a**). The protein functionalized NPs (CoFerrite2@FITC-BSA) spectrum showed apart from the main peaks of OAm, the characteristic peaks of FITC-BSA located at 750-1250 cm^{-1} region too, while the peaks at 700 cm^{-1} attributed to the spinel structure also appeared. In order to exclude the possibility of protein adsorption onto the NPs, a blank experiment was conducted. Experimentally, the reaction was done without UV light irradiation at 365 nm that would normally trigger the radical coupling reaction.

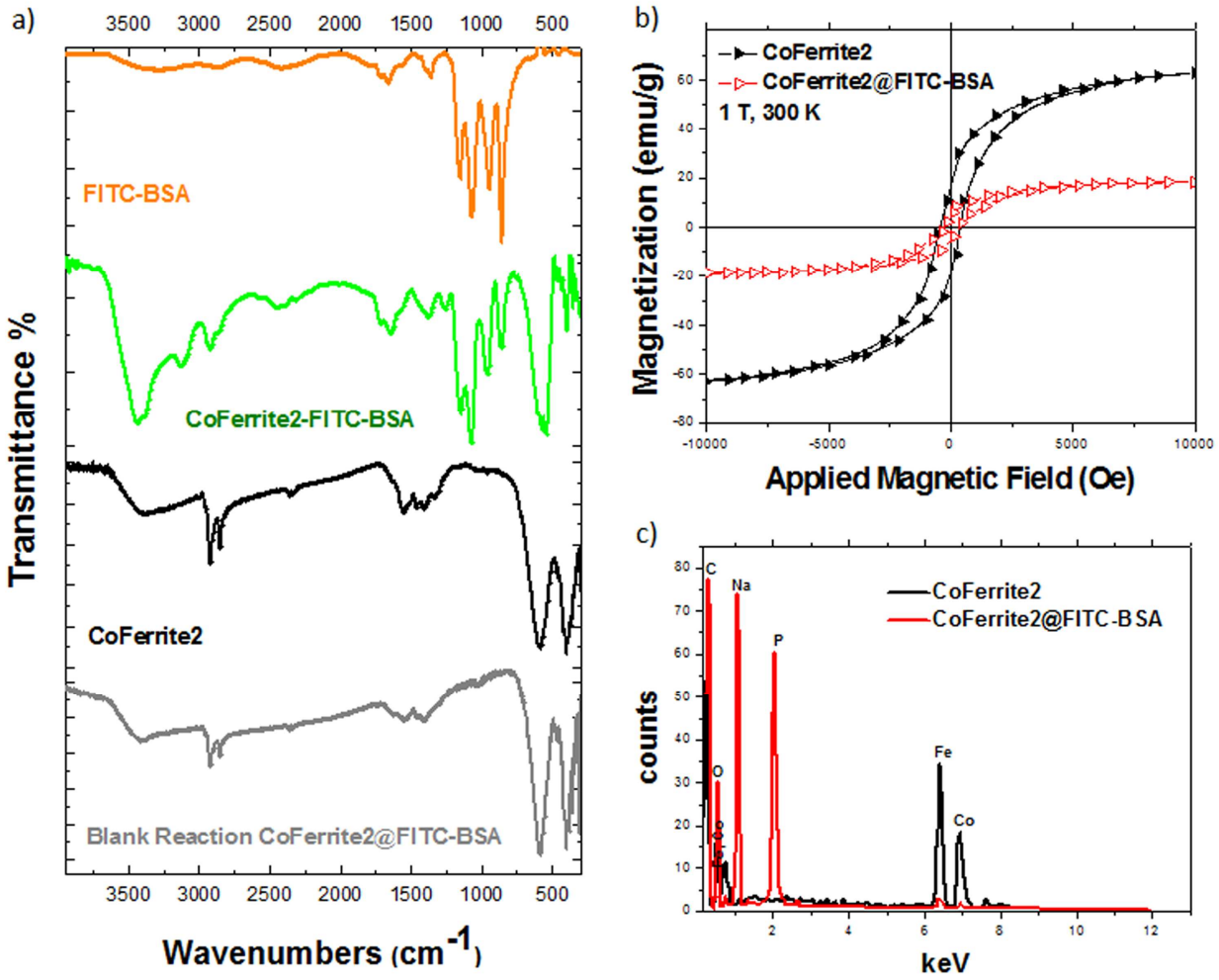

Figure 5. a) IR spectra of free FITC-BSA (orange), CoFerrite2-FITC-BSA (green), CoFerrite2 (black), product of blank reaction (grey) b) Magnetic measurements without organic component correction and c) Elemental analysis of CoFerrite2 and CoFerrite2-FITC-BSA

No evidence of FITC-BSA conjugate was observed in the IR spectrum after the purification of the blank sample (**Figure 5a**). In addition, EDS analysis (**Figure 5c**) indicates the presence of FITC-BSA by the extra peaks of sodium and phosphorus as well as by the increase of oxygen and carbon peaks. The characteristic decrease of iron and cobalt peaks indicates the dominant fluorophore conjugate in the sample.

Furthermore, an estimation of albumin's concentration functionalized on the surface of NPs was achieved by Bradford analysis[40] and the amount of albumin was calculated, 1.14 µg/L. Following the coupling of FITC-BSA on NPs, the fluorescence properties of the dye, isothiocyanate fluorescein, were also altered (**Figure 6a**).

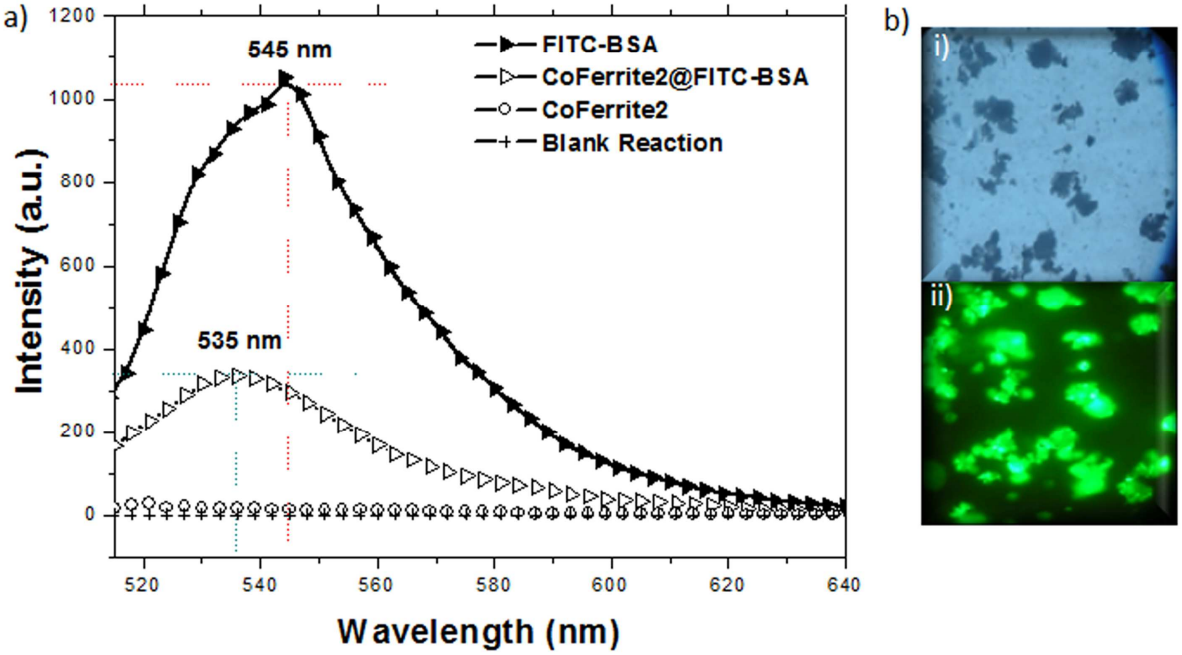

Figure 6. a) Fluorescence measurements of FITC-BSA (-▶-), CoFerrite2@FITC-BSA (-▷-), CoFerrite2(-◇-), product of blank reaction (-+-), b) Images of CoFerrite2@FITC-BSA i) under an optical microscope and ii) under fluorescence light.

A shift of 10 nm of the CoFerrite2@FITC-BSA NPs emission (λ_{em} = 535 nm) was observed when compared to that of the FITC-BSA (λ_{em} = 545 nm) while a clear decrease of fluorescence intensity was also noticed. Furthermore, magnetic features of the sample were clearly modified after FITC-BSA functionalization. A comparison of the hysteresis loops of the as prepared CoFerrite2 NPs and the functionalized CoFerrite2@FITC-BSA is given in **Figure 5b**. A significant decrease of the net magnetization was observed, from 63.04 emu/g (M_s of CoFerrite2 without correction from TGA data, H_c=370 Oe) to 18.4 emu/g (H_c=343 Oe) attributed to the conjugation of the large molecular weight diamagnetic molecule (FITC-BSA) onto the NPs.

^{1}H-NMR solution spectroscopy was proved a useful tool to certify the presence of OAm coating on $CoFe_2O_4$ NPs as well as the conjugation of FITC-BSA. ^{1}H-NMR spectra of pure OAm, CoFerrite2, CoFerrite2@FITC-BSA and pure FITC-BSA in $CDCl_3$ are given in **Figure 7** for comparison. The characteristic resonances of vinyl (a-H), allyl (c-H), methylene (b-H) and (e-H), methyl (g-H) and amine group (f-H) protons can be distinguished at 5.38, 2.2, 2.02, 1.3, 0.83 and 1.2 ppm (**Fig 7 ii**) respectively and they are obviously shifted compared to the spectrum of pure OAm (**Fig 7 i**) while due to the ferrimagnetic origin of $CoFe_2O_4$ NPs, peaks are broad as expected[41] especially for the vinyl (a-H) protons (magnified region). In the case of CoFerrite2@FITC-BSA (**Fig 7 iii**), due to the larger coating and smaller percentage of metal NPs the spectrum appears to have sharper peaks[41] with the dominant characteristic resonances of FITC-BSA (**Fig 7 iii and iv**).

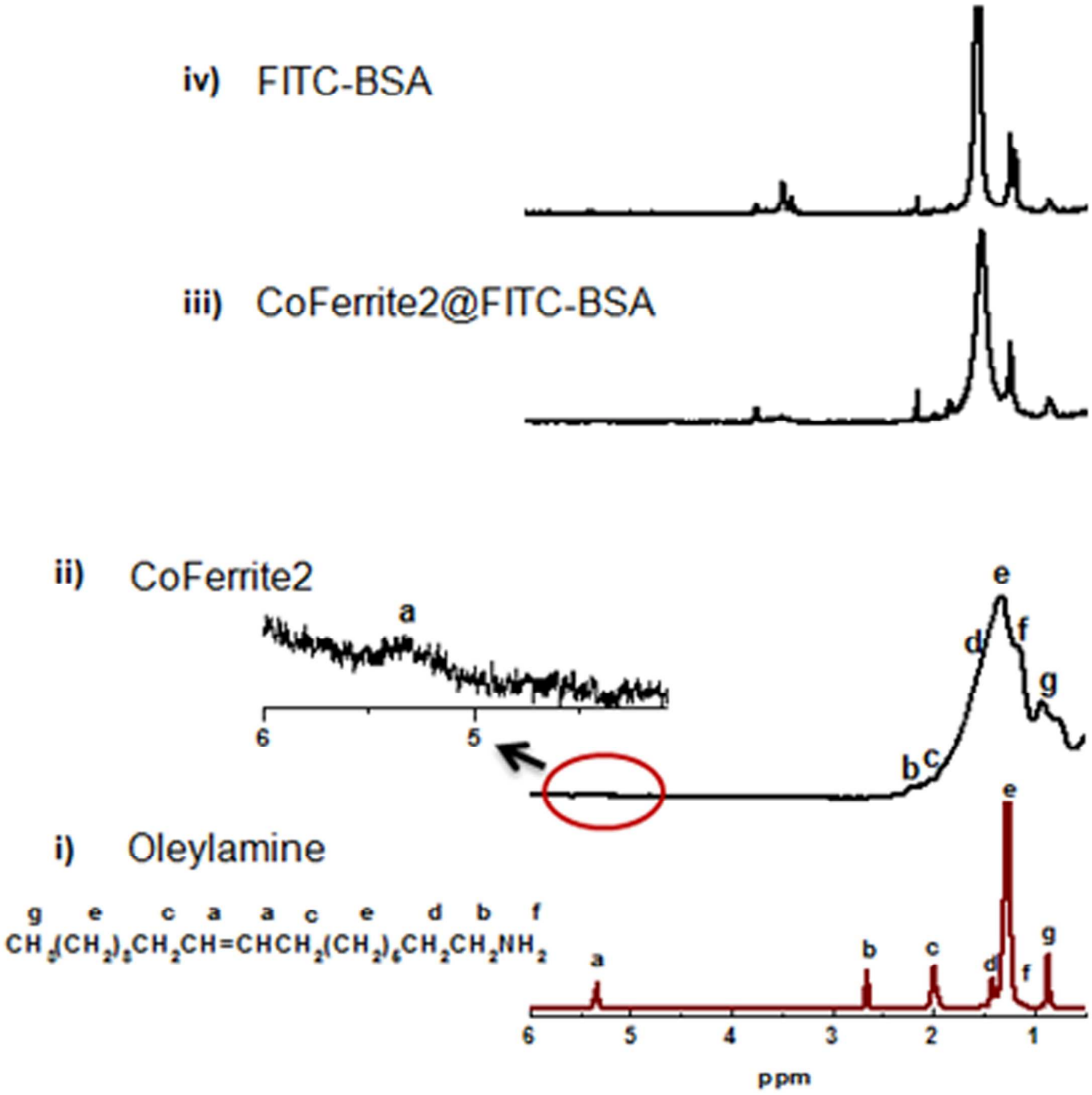

Figure 7. ^{1}H-NMR spectra of i) pure OAm, ii) CoFerrite2, iii) CoFerrite2@FITC-BSA and iv) pure FITC-BSA

After all it can be stated that the functionalization has been achieved through the establishment of a covalent bond between FITC-BSA and the reactive double bonds of the OAm coating onto the magnetic NP surface. A schematic representation of thiol-ene "click" reaction is depicted in **Scheme 1**.

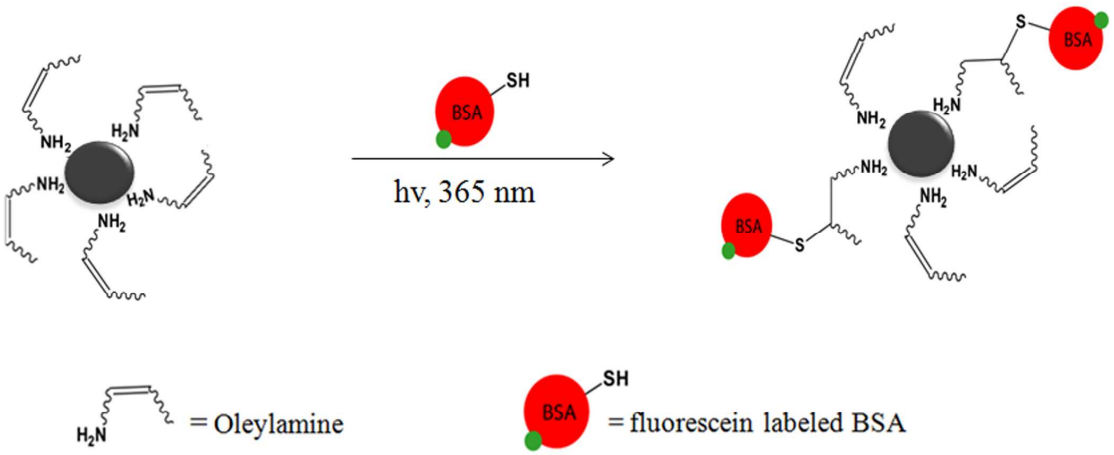

Scheme 1. Schematic representation of the thiol-ene "click" reaction

Cell viability assessments

CoFerrite2@FITC-BSA NPs were incubated with a number of cancer and non-cancer human cell lines at different concentrations (**Figure 8**, **Figure 4S**).

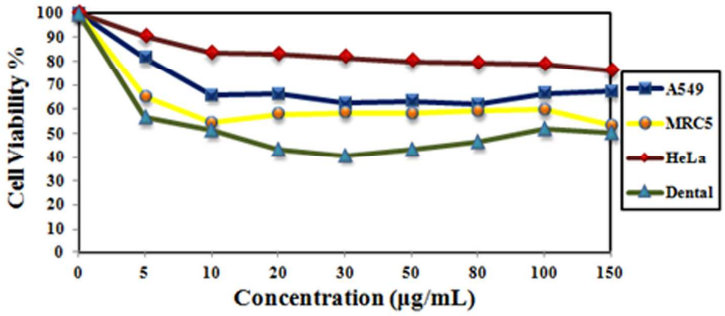

Figure 8. Dose-effect survival plots of NPs, against a panel of human cancer and normal cell lines, 48 h incubation. Each point represents a mean of three replicate wells.

In particular, after 48 h cell exposure to the NPs the assessed cell viability-based on their mitochondrial activity-was not affected; the percentage of lowest cell viability in relation to NPs concentration is given in **Table 1S**. Dental MSCS was found to be more sensitive (40.83% viability), in contrast to HeLa (75.95%). Another noteworthy observation is that cancer cells (HeLa, A549), seem to be more resistant than the non-cancer (MRC5, Dental MSCS). Additionally, pure OAm has been tested by MTT assays on cancer (HeLa) and non-cancer (MRC5) cell lines (**Fig.5S**) and toxicity was found concentration dependent in the specific conditions. Taking into account that OAm participates in the system in a very low concentration, no evidence of cytotoxic effect due to the surfactant can be acknowledged. Leaching tests were performed for the highest concentration of NPs (150 µg/mL), in three different media: H_2O, culture medium (DMEM), and DMEM with fetal bovine serum (FBS), after 48 h incubation and showed that the released iron concentration [Fe], is 3.56, 76.8 and 113.2 ($x10^{-3}$µg/mL) for each system respectively (data by GFAAS). The low release of Fe ions indicates that cytotoxic effect is correlated with the nanosize effect and not with a leaching process of Fe ions.[42]

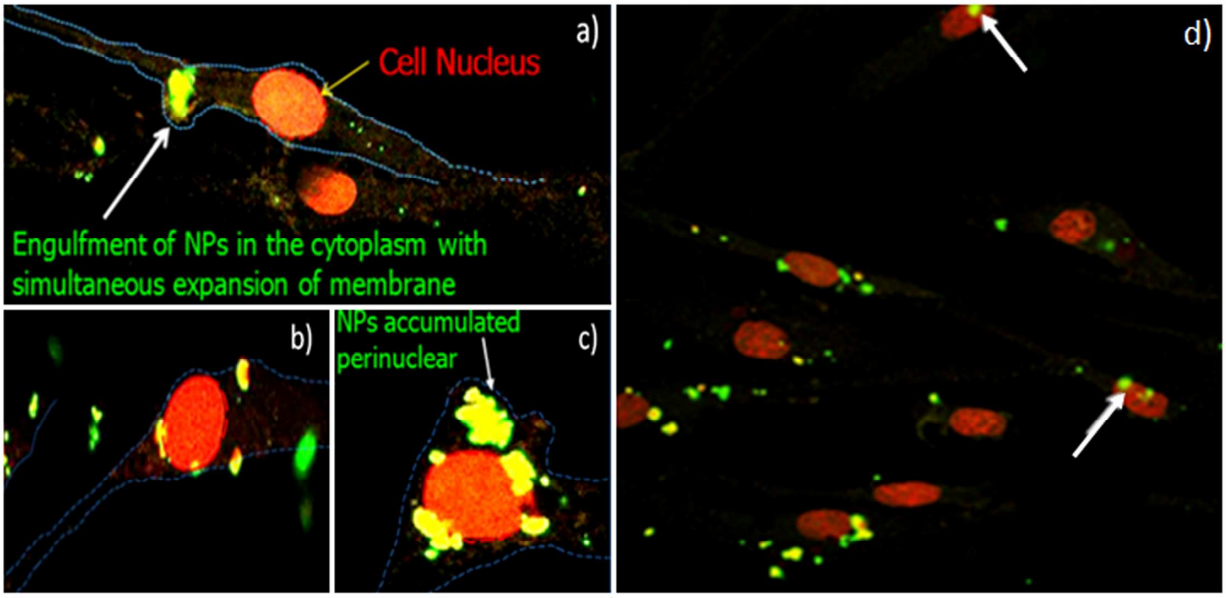

Figure 9. Cellular localization of NPs (green staining) after incubation with Dental MSCS cells for 48 h. Cell nuclei (red staining). a) Engulfment of NPs in the cytoplasm with simultaneous expansion of the membrane; b) and c) NPs are located in the perinuclear membrane. d) Vertical scans of the cells showed whether the NPs inserted the cells (same level with the cell) or if they were outside, on the surface of the cell membrane (white arrows).

PI staining and confocal microscopy investigation

The nuclei staining by the PI method in conjunction with confocal laser microscopy indicated the NPs' route inside the cell membranes. Cellular localization of the NPs after their incubation with Dental MSCS cells for 48 hours (**Figure 9**) showed that NPs entered the cell membranes and were localized close to them (**Figure 9c**) provoking a membrane expansion (**Figure 9a**) and were further accumulated perinuclear (**Figure 9b** and **c**) without entering the nuclei, at least under the conditions used. The main observed phenotype was that of **Figure 9a** and **b**, and these aggregations in the perinuclear region are probably a result of endosomal fusions, combining several vesicles with small aggregates. Additionally, vertical scans of the cells were performed in order to show that the NPs inserted the cells and were not located outside, on the surface of the cell membrane (**Figure 9d** and **Figure 6S**).

The interactions of the NPs with the cells have been an intensive area of many ongoing studies, which aim to elucidate the specific interactions between the NPs and cell constituents as well. Regarding the cell "uptake" of NPs, two endocytic pathways have been proposed, the clathrin-mediated endocytosis (CME) and macropinocytosis.[43] Namely a receptor mediated and a non-receptor mediated mechanism, respectively. In particular, CME is responsible for internalization of several activated signaling receptors and also for the uptake of nutrients, while the second observed pathway is a macropinocytosis which is a non receptor mediated endocytic mechanism that enables the internalization of larger volumes and also particles, into nonphagocytic cells. Once internalized, NPs are mostly reported to be present in vesicles[44] that travel toward the perinuclear region[45] or are colocalized with lysosomes and late endosomes[46]. Specifically, for $CoFe_2O_4$ NPs there is no information regarding their placement within the nucleus and that is in consistency with our addressed results. However, their biological

investigation is imperative since their implementation requires knowledge on the molecular level. Regarding their cytotoxicity, it is determined by several factors including both cell physiology and NPs properties as size, material, surface characteristics and shape as well.[47] This particular suggestion is further corroborated by our results, which showed a clear difference of toxicity between the cancer and non-cancer cells studied as well. However it is not clear whether it is an effect of cell membrane penetration or some other factors localized inside the cell.

Conclusions

To the best of our knowledge, it is the first time in the frame of this paper that OAm is used as the primary component in the solvothermal synthesis of $CoFe_2O_4$ NPs and serves as the foundation of the NP-surface functionalization, a precondition for the subsequent NP-evaluation in theranostics. OAm is an inexpensive and easily handled surfactant while as a liquid long chain amine with a high boiling point and reducing ability there is no need of extra solvent and yet survives the harsh solvothermal conditions. By differentiating the filling capacity of the closed bomb, truncated 10.7 nm were isolated with improved magnetization Ms=87.5 emu/g. The ability to tune solubility by altering surface chemistry with the charged molecule CTAB gave rise to measure relaxivity properties. The CTAB modified $CoFe_2O_4$ NPs gave comparable results with literature data as T_2 agents and in case of the spherical, 9 nm NPs, a large effect on relaxivity of water protons (r_2=553 $mM^{-1}s^{-1}$) was observed. Additionally, the as prepared NPs readily became fluorescent probes via a thiol-ene "click" reaction with the fluorescein isothiocyanate labeled bovine serum albumin under UV irradiation and further expansion to active biomolecules can be foreseen. The labeled NPs interacted with cancer (HeLa, A549) and non-cancer (MRC5, Dental MSCS) cell lines and cell viability was estimated. A clear difference of toxicity between the cancer and non-cancer cells was observed while they showed low cytotoxicity in living cells. Confocal laser microscopy showed that NPs entered the cell membranes and localized close to them provoking a membrane expansion and were further accumulated perinuclear without entering the nuclei, at least under the conditions used.

Acknowledgements

The authors C. Dendrinou – Samara and V. Georgiadou are grateful for the financial support of the European Union (European Social Fund – ESF) and Greek national funds through the Operational Program "Education and Lifelong Learning" of the National Strategic Reference Framework (NSRF) - Research Funding Program: Thales. Investing in knowledge society through the European Social Fund. All the authors would like to thank E. Kasotakis and the "TEM-team" platform (iBiTec-S/SB2SM) for technical assistance.

References

1 A. Goldman in *Modern Ferrite Technology*, Springer Science+Business Media, Inc. New York, 2006, ch. 5, pp. 71-109

2 S. Noh, W. Na, J. Jang, J-H. Lee, E. J. Lee, S. H. Moon, Y. Lim, J-S. Shin and J. Cheon, *Nano Lett.*, 2012, **12**, 3716-3721

3 J. L. Corchero and A. Villaverde, *Trends Biotechnol.*, 2009, **27**, 468-476; T. Osaka, T. Matsunaga, T. Nakanishi, A. Arakaki, D. Niwa and H. Iida, *Anal. Bioanal. Chem.*, 2006, **384**, 593-600; S. A. Corr, Y. P. Rakovich and Y. K. Gun'ko, *Nanoscale Res. Lett.*, 2008, **3**, 87-104

4 Y. Wang, C. Xu and H. Ow, *Theranostics*, 2013, **3,** 544-560; S. Amiri and H. Shokrollahi, *Mater. Sci. Eng., C*, 2013, **33**, 1-8

5 H. M. Joshi, *J. Nanopart. Res.*, 2013, **15**, 1235 (pp. 1-19)

6 D. Peddis, F. Orrù, A. Ardu, C. Cannas, A. Musinu and G. Piccaluga, *Chem. Mater.*, 2012, **24**, 1062-1071; X. Jia, D. Chen, X. Jiao, T. He, H. Wang and W. Jiang, *J. Phys. Chem. C,* 2009, 112, 911-917; K. P. Naidek, F. Bianconi, T. C. da Rocha, D. Zanchet, J. A. Bonacin, M. A. Novak, Md. Vaz and H. Winnischofer, *J. Colloid Interf. Sci.*, 2011, **358**, 39-46; A. Thampi, K. Babu and S. Verma, *J. Alloy. Compd.*, 2013, **564**, 143-150

7 Y. Ma, J. Zeng, W. Li, M. McKiernan, Z. Xe and Y. Xia, *Adv Mater.*, 2010, **22**, 1930; M. Menelaou, K. Georgoula, K. Simeonidis and C. Dendrinou-Samara, *Dalton Trans.*, DOI: 10.1039/C3DT52860J.

8 S. Mourdikoudis and L. M. Liz-Marzán, *Chem. Mater.*, 2013, **25**, 1465-1476

9 L. Perez-Mirabet, E. Solano, F. Martınez-Julian, R. Guzman, J. Arbiol, T. Puig, X. Obradors, A. Pomar, R. Yanez, J. Ros and S. Ricart, *Mater. Res. Bull.*, 2013, **48**, 966-972; J. Mohapatra, A. Mitra, D. Bahadur and M. Aslam, *Cryst. Eng. Commun*., 2013, **15**, 524-532

10 R. D. Rutledge, C. L. Warner, J. W. Pittman, R. S. Addleman, M. Engelhard, W. Chouyyok and M. G. Warner, *Langmuir,* 2010, **26**, 12285-12292; A. K. Tucker-Schwartz, R. A. Farrell and R. L. Garrell, *J. Am. Chem. Soc.*, 2011, **133**, 11026-11029; K. Y. Van Berkel and C. J. Hawker, *J. Polym. Sci. Pol. Chem.*, 2010, **48**, 1594-1606

11 Y. Tian, B. Yu, X. Li and K. Li, *J. Mater. Chem.*, 2011, **21**, 2476-2481

12 C. Maison, H. Horstmann and S. D. Georgatos, *J. Cell Biol.*, 1993, **123**, 1491-1505

13 T. Mosmann, *J. Immunol. Methods.*, 1983, **65**, 55-63

14 G. Zhang, P. He, X. Ma Y. Kuang, J. Liu, X. Sun, *Inorg. Chem.*, 2012, **51**, 1302-1308

15 G. Demazeau, *Z. Naturforsch. B.*, 2006, **61b**, 799-807

16 M. Niederberger, G. Garnweitner, *Chem. Eur. J.*, 2006, **12**, 7282-7302

17 Z. Wei, T. Xia, J. Ma, W. Feng, J. Dai, Q. Wang and P. Yan, *Mater. Charact.*, 2007, 58, 1019-1024

18 N. Shukla, C. Liu, P. M. Jones and D. Weller, *J. Magn. Magn. Mater.*, 2003, **266**, 178-184

19 Z. Xu, C. Shen, Y. Hou, H. Gao and S. Sun, *Chem. Mater.*, 2009, **21**, 1778-1780; J. L. Zhang, R. S. Srivastava and R. D. K. Misra, *Langmuir,* 2007, **23**, 6342-6351

20 R. D. Waldron, *Phys. Rev.*, 1955, **99**, 1727-1735

21 I. Sharifi, H. Shokrollahi, M. M. Doroodmand and R. Safi, *J. Magn. Magn. Mater.*, 2012, **324**, 1854-1861

22 E. Solano, L. Perez-Mirabet, F. Martinez-Julian, R. Guzman, J. Arbiol, T. Puig, X. Obradors, R. Yanez, A. Pomar, S. Ricart and J. Ros, *J. Nanopart. Res.*, 2012, **14**, 1034 (pp. 1-15)

23 H. M. Joshi, Y. P. Lin, M. Aslam, P. V. Prasad, E. A. Schultz-Sikma, R. Edelman, T. Meade and V. P. Dravid, *J. Phys. Chem. C,* 2009, **113**, 17761-17767

24 M. Y. Rafique, L. Pan, Q. Javed, M. Z. Iqbal and L. Yang, *J. Nanopart. Res.*, 2012, **14**, 1189 (pp. 1-12)

25 D. Elwell and R. Parker, *Philos. Mag.*, 1964, **10,** 253-261

26 C. E. R. Torres, F. Golmar, M. Ziese, P. Esquinazi and S. P. Heluani, *Phys. Rev. B*, 2011 **84,** 064404 (pp. 1-5)

27 L. Suber and D. Peddis in *Magnetic nanomaterials* ed. C. Kumar WILEY-VCH Verlag GmbH & Co. KGaA, Weinheim, 2009, Vol.4, ch. 12, pp. 431-487
28 J. C. Slonczewski, *Phys. Rev.*, 1958, **110**, 1341–1348
29 D. Peddis, C. Cannas, A. Musinu, and G. Piccaluga, *Chem. Eur. J.*, 2009, **15**, 7822-7829
30 Q. A. Pankhurst, J. Connolly, S. K. Jones and J. Dobson, *J. Phys. D Appl. Phys.*, 2003, **36**, R167-R181
31 Y-w. Jun, Y-M. Huh, J-s. Choi, J-H. Lee, H-T. Song, S. Kim, S. Yoon, J-S. Shin, J-S. Suh and J. Cheon, *J. Am. Chem. Soc.*, 2005, **127**, 5732-5733; Y. K. Gun'ko and D. F. Brougham in *Magnetic nanomaterials* ed. C. Kumar WILEY-VCH Verlag GmbH & Co. KGaA, Weinheim, 2009, Vol.4, ch. 4, pp. 121-128
32 M. De, S. S. Chou, H. M. Joshi and V. P. Dravid, *Adv. Drug Deliver. Rev.*, 2011, **63**, 1282-1299
33 S. L. C. Pinho, G. A. Pereira, P. Voisin, J. Kassem, V. Bouchaud, L. Etienne, J. A. Peters, L. Carlos, S. Mornet, C. F. G. C. Geraldes, J. Rocha and M-H. Delville, *ACS Nano,* 2010, **4**, 5339-5349
34 M. Aslam, E. A. Schultz, T. Sun, T. Meade and V. P. Dravid, *Cryst. Growth Des.*, 2007, **7**, 471-475
35 D. W. Hwang, I. C. Song, D. S. Lee and S. Kim, *Small*, 2010, **6**, 81-88; T-J. Yoon, K. N. Yu, E. Kim, J. S. Kim, B. G. Kim, S-H. Yun, B-H. Sohn, M-H. Cho, J-K. Lee and S. B. Park, *Small*, 2006, **2**, 209-215
36 O. M. Koo, I. Rubinstein and H. Onyuksel, *Nanomed-Nanotechnol.*, 2005, **1**, 193-212
37 X. Liu, M. D. Kaminski, H. Chen, M. Torno, L. Taylor and A. J. Rosengart, *J. Control. Release*, 2007, **119**, 52-58
38 J. Amici, P. Allia, P. Tiberto and M. Sangermano, *Macromol. Chem. Phys.*, 2011, **212**, 1629-1635
39 C. Hoyle, T. Y. Lee and T. Roper, *J. Polym. Sci. Pol. Chem.*, 2004, **42**, 5301-5338
40 M. M. Bradford, *Anal. Biochem.*, 1976, **72**, 248-254
41 C. Cannas, A. Musinu, A. Ardu, F. Orru, D. Peddis, M. Casu, R. Sanna, F. ANgius, G. Diaz and G. Piccaluga, *Chem. Mater.*, 2010, **22**, 3353-3361; A. L. Willis, N. J. Turro, S. O'Brien, *Chem. Mater.*, 2005, **17**, 5970-5975
42 L. Horev-Azaria, G. Baldi, D. Beno, D. Bonacchi, U. Golla-Schindler, J. C. Kirkpatrick, S. Kolle, R. Landsiedel, O. Maimon, P. N. Marche, J. Ponti, R. Romano, F. Rossi, D. Sommer, C. Uboldi, R. E. Unger, C. Villiers and R. Korenstein, *Particle and Fibre Toxicology,* 2013, **10**, 32 (pp. 1-17)
43 V. B. Bregar, J. Lojk, V. Sustar, P. Veranic and M. Pavlin, *Int. J. Nanomed.*, 2013, **8**, 919-931
44 C. Wilhelm, F. Gazeau, J. Roger, J.N. Pons and J-C. Bacri, *Langmuir,* 2002, **18**, 8148-8155
45 A. Moore, R. Weissleder and Jr.A. Bogdanov, *J. Magn. Reson. Imaging,* 1997, **7**, 1140-1145
46 P. Marmorato, G. Ceccone, A. Gianoncelli, L. Pascolo, J. Ponti, F. Rossi, M. Salome, B. Kaulich and M. Kiskinova, *Toxicol. Lett.*, 2011, **207**, 128-136
47 N. Lewinski, V. Colvin and R. Drezek, *Small,* 2008, **4**, 26-49

Table of contents

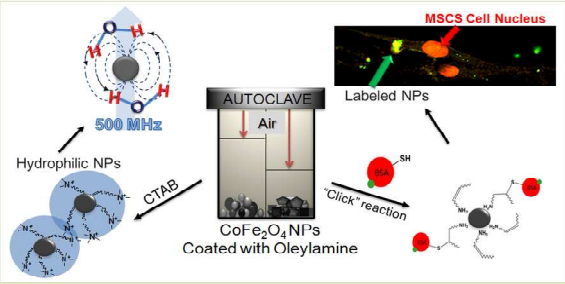

Solvothermally synthesized oleylamine-coated $CoFe_2O_4$-NPs, exhibiting NMR relaxometric properties, were modified by click chemistry and interacted with cell lines.